Talanta 134 (2015) 607–618

Contents lists available at ScienceDirect

Talanta

journal homepage: www.elsevier.com/locate/talanta

Generation of non-multilinear three-way voltammetric arrays by an electrochemically oxidized glassy carbon electrode as an efficient electronic device to achieving second-order advantage: Challenges, and tailored applications

Ali R. Jalalvand [a,b], Mohammad-Bagher Gholivand [a,*], Hector C. Goicoechea [b], Thomas Skov [c]

[a] Department of Analytical Chemistry, Faculty of Chemistry, Razi University, Kermanshah 671496734, Iran
[b] Laboratorio de Desarrollo Analítico y Quimiometría (LADAQ), Cátedra de Química Analítica I, Universidad Nacional del Litoral, Ciudad Universitaria, CC 242 (S3000ZAA), Santa Fe, Argentina
[c] Quality & Technology, Department of Food Science, Faculty of Science, University of Copenhagen, Copenhagen, Denmark

ARTICLE INFO

Article history:
Received 23 October 2014
Received in revised form
28 November 2014
Accepted 29 November 2014
Available online 11 December 2014

Keywords:
Second-order advantage
Paracetamol
Norepinephrine
Uric acid
Simultaneous quantification
Uncalibrated interference.

ABSTRACT

For the first time, several second-order calibration models based on artificial neural network-residual bilinearization (ANN-RBL), unfolded-partial least squares-RBL (U-PLS/RBL), multidimensional-partial least squares-RBL (N-PLS/RBL), multivariate curve resolution-alternating least squares (MCR-ALS), and parallel factor analysis 2 (PARAFAC2) were used to exploiting second-order advantage to identify which technique offers the best predictions for the simultaneous quantification of norepinephrine (NE), paracetamol (AC), and uric acid (UA) in the presence of pteroylglutamic acid (FA) as an uncalibrated interference at an electrochemically oxidized glassy carbon electrode (OGCE). Three-way differential pulse voltammetric (DPV) arrays were obtained by recording the DPV signals at different pulse heights. The recorded three-way arrays were both non-bilinear and non-trilinear therefore, the observed shifts in the recorded DPV data were corrected using correlation optimised warping (COW) algorithm. All the algorithms achieved the second-order advantage and were in principle able to overcome the problem of the presence of unexpected interference. Comparison of the performance of the applied second-order chemometric algorithms confirmed the more superiority of U-PLS/RBL to resolve complex systems. The results of applying U-PLS/RBL for the simultaneous quantification of the studied analytes in human serum samples were also encouraging.

1. Introduction

The recent developments in multi-dimensional analytical instrumentation and data collection are producing data arrays of increasing complexity, which are particularly useful for quantitative analysis in complex mixtures. It is apparent that this progress towards multi-way data offers theoretical and practical advantages from an analytical point of view [1–3]. For example, whereas zeroth-order univariate calibration cannot detect sample components producing an interfering signal, first-order calibration, which operates using a vector of data per sample, may compensate for these potential interferents, provided they are included in the calibration set, a property known as the "first-order advantage" [4]. Going one step further, second-order data lead to three-way arrays which can be uniquely decomposed, allowing relative concentrations and profiles of the individual components in the different domains to be extracted directly. In this way, analytes can

Abbreviations: ANN, artificial neural network; RBL, residual bilinearization; U-PLS, unfolded-partial least squares; N-PLS, multidimensional-partial least squares; MCR-ALS, multivariate curve resolution-alternating least squares; PARAFAC2, parallel factor analysis 2; NE, norepinephrine; AC, paracetamol; UA, uric acid; FA, pteroylglutamic acid; OGCE, oxidized glassy carbon electrode; COW, correlation optimised warping; UPW, ultrapure water; EIS, electrochemical impedance spectroscopy; ATLD, alternating trilinear decomposition; SWATLD, self-weighted ATLD; APTLD, penalized ATLD; GRAM, generalized rank annihilation method; DTLD, direct trilinear decomposition; BLLS, bilinear least-squares; EFA, evolving factor analysis; AFOM, analytical figures of merit; NAS, net analyte signal; LOD, limit of detection; SEL, selectivity; SEN, sensitivity; SVD, singular value decomposition; OLS, ordinary least squares; EJCR, elliptical joint confidence region; SIMPLISMA, simple interactive self-modeling mixture analysis.

* Corresponding author. Tel.: +98 831 4274557; fax: +98 831 4274559.
E-mail addresses: mbgholivand2013@gmail.com, mbgholivand@yahoo.com (M.-B. Gholivand).

http://dx.doi.org/10.1016/j.talanta.2014.11.066
0039-9140/

be quantified even in the presence of unknown interferents which are not included in the calibration set. This property has been generally recognized as the "second-order advantage", a term coined in 1994 [4], although the first experimental demonstration of this advantage was reported in 1978, when perylene was determined in mixtures with anthracene, by suitable processing of fluorescence excitation-emission matrix data [5]. Second-order data for a given sample can be easily produced in a variety of ways, either in a single instrument or by resorting to instrument hyphenation.

Multi-way analysis allows direct separation of the measured signals into the underlying contributions from individual analytes. In second-order domain, three-way data generates a matrix from a single chemical sample. The processing of second-order data have attracted the attention of chemometricians in recent years for a variety of reasons: (1) they are now abundantly produced by modern analytical instruments, (2) they show peculiar mathematical characteristics which distinguish them from first order data, and (3) they provide analytical chemists with the important second-order advantage, an intrinsic property which permits analyte quantitation in the presence of unexpected sample components (i.e., components not present in the calibration set of samples) [6].

Norepinephrine (NE) is an important catecholamine neurotransmitter and is secreted by the adrenal medulla. It is released as a metabotropic neurotransmitter from nerve endings in the sympathetic nervous system and some areas of the cerebral cortex. Many diseases are related to changes of its concentration [7]. Thus the quantitative determination of NE in biological fluids for medical control and in pharmaceutical formulations for quality control analysis is important. Besides various methods such as spectrophotometry [8], capillary electrophoresis [9], gas chromatography [10] and high-performance liquid chromatography [11]; electrochemical methods have also been employed for detection of NE [12–15].

Paracetamol (AC) is the most extensively employed drug as pain reliever and fever reducer. However, overdoses of AC cause liver and kidney damage and may lead to death [16,17]. Several methods have been used for the determination of AC including spectrophotometry [18], chromatographic methods [19] and electroanalysis by modified electrodes [20–24].

Uric acid (UA or 2,6,8-trihydroxypurine) is the primary end product of purine metabolism. Physiological UA serum level is in the range of 4.1–8.8 mg (per 100 mL) and with urinary excretion typically in the range of 250–750 mg (per 100 mL). Its abnormal concentration level in the human body will lead to several diseases such as hyperuricaemia, gout, leukemia, lesch-nyhan syndrome and pneumonia [25]. Therefore, the development of a rapid, selective and simple method is very important for its determinations in routine analysis. Due to the advantages of low cost, fast response, simple instrumentation, high sensitivity, facile miniaturization, and low power requirement, numerous voltammetric methods for determination of UA have been developed [26–28].

AC administration increases brain serotonin levels [29] and serotonin is known to play a role in NE release in the brain [30]. Also, pteroylglutamic acid (FA) works primarily in the brain and nervous system and is necessary for the synthesis of NE and serotonin in the nervous system. Also, some substances like nonsteriodal anti-inflammatory drugs such as AC can inhibit FA from being absorbed or used by the body. Likewise, when taken for long periods of time, AC can also increase the need for FA [31]. On the other hand UA is naturally present in the body therefore, after drugs ingestion NE, AC, UA, and FA can be found in biological fluids. FA is one of the usual interferences in the simultaneous determination of NE, AC, and UA because the oxidation peak potential for FA was very close to those of NE, AC, and UA therefore, FA was considered as interference in the simultaneous determination of NE, AC, and UA.

In the present study, we introduced an efficient electroanalytical method based on exploiting second-order advantage from DPV data for the simultaneous quantification of AC, NE, and UA in the presence of FA as uncalibrated interference. Glassy carbon electrode (GCE) is made up of special type of carbon which fabricated by pyrolsis of polymer resin exhibits good electrical conductivity with well-defined surfaces. The chemical and electrochemical pretreatment shows significant changes in physical and electrochemical properties of GCE. In particular, electrochemical activation of GCE results in the generation of surface functional groups which could be used as capacitor electrodes. By the use of GCE we weren't able to determine low concentrations of the analytes of interest therefore, this problem prompted us to use an electrochemically oxidized GCE (OGCE) for quantifying the analytes of interest. As expected, electrochemical oxidation of GCE increases porosity of GCE and improves electron transfer kinetic between analyte and electrode. Because of the non-linear behavior of the recoded second-order data, three hybrid second-order algorithms including ANN-RBL, U-PLS/RBL, and N-PLS/RBL were used and their prediction performance was compared with MCR-ALS and PARAFAC2. The observed shifts in the recorded data were corrected by the use of COW algorithm. Finally, according to the obtained results, U-PLS/RBL was chosen as the best algorithm for the simultaneous quantification of the studied analytes in human serum samples as experimental cases.

2. Theoretical and experimental considerations

2.1. Theoretical details

2.1.1. Generating second-order DPV data

In this work, the pulse height (ΔE) in DPV was changed to obtain electrochemical second-order data. The theory behind the proposed procedure will be briefly discussed. The current signal intensity in DPV can be obtained using the following equations [32]:

$$\delta_i = \frac{n\mathrm{FAD}_O^{1/2}C_O^*}{\pi^{1/2}(\tau-\tau')^{1/2}}\left[\frac{P_A(1-\sigma^2)}{(\sigma+P_A)(1+P_A\sigma)}\right] \quad (1)$$

$$P_A = \xi\exp\left[\frac{n\mathrm{F}}{\mathrm{RT}}\left(E+\frac{\Delta E}{2}-E^{0'}\right)\right] \quad (2)$$

$$\sigma = \exp\left(\frac{n\mathrm{F}}{\mathrm{RT}}\frac{\Delta E}{2}\right) \quad (3)$$

$$\xi = \left(\frac{D_O}{D_R}\right)^{1/2} \quad (4)$$

where ΔE is the pulse height and other symbols have their conventional meanings. For a typical electrochemical reaction, a data vector can be obtained by sweeping the potential at constant ΔE and τ. Applying a different ΔE and sweeping potential at the constant τ, will produce different data vectors, i.e., sweeping the potential and applying different pulse heights (ΔEs) at a constant pulse duration in DPV produces a non-bilinear second-order data.

2.1.2. Second-order calibration algorithms

Second-order data can be processed by a variety of algorithms for analyte quantitation. Those classified as trilinear are: (1) parallel factor analysis (PARAFAC) [33], (2) different versions of alternating trilinear decomposition (ATLD) [34], such as self-weighted ATLD (SWATLD) [35] and penalized ATLD (APTLD) [36], (3) generalized

rank annihilation method (GRAM) [37], (4) direct trilinear decomposition (DTLD) [38], and (5) bilinear least-squares combined with residual bilinearization (BLLS/RBL) [39,40]. All these methods assume an intrinsic mathematical model in which the profiles of all components are the same in all samples.

On the other hand, there are algorithms allowing for deviations of multi-linearity, which may be able to model retention time shifts, such as: (1) multivariate curve resolution coupled-alternating least squares (MCR-ALS) [41] and (2) PARAFAC2, a variant of PARAFAC which allows profile variations in one of the data dimensions from sample to sample [42]. In MCR-ALS, the basis of the successful data resolution is the building of an augmented matrix, placing all calibration and test data matrices adjacent to each other in the pulse height direction. In this way, the time profile for a given component is allowed to vary from sample to sample. In the case of PARAFAC2, a relaxed PARAFAC model is employed which allows profiles to vary in one of the data dimensions from sample to sample. PARAFAC2 provides similar information to its trilinear counterpart, except that the pulse height profile is not common to all samples. What is important, however, is that it renders analyte scores which are also used to predict its concentration in the unknowns by pseudo-univariate calibration. PARAFAC2 admits lesser constraints to be imposed during the least-squares fit in comparison with the full range of constraints which are available for MCR-ALS in both data dimensions [43]. Thus, in certain complex cases the latter methodology may produce results which are better from the point of view of their physical interpretability, analytical accuracy and precision.

Other potentially useful second-order calibration methods are unfolded partial least-squares (U-PLS) [44], multi-way PLS (N-PLS) [45], and ANN-RBL [46], and should be combined with RBL if the second-order advantage is to be achieved [47–52]. These PLS algorithms intend to model the profile variations by incorporating a flexible latent structure in regressing the data. However, their full potentiality regarding the modeling of pulse height variations is still a matter of debate. In any case, PLS models do not provide chemical recognizable information, because they internally work with abstract loadings, which are linear combinations of true profiles.

2.1.3. Pre-treatments of recorded data

Besides the problem arising from the presence of severely overlapping analyte profiles, in the present study two additional complications may occur: (1) interactions among analytes and the background interferents present in the serum, which may cause signal changes in comparison with pure analyte profiles, and (2) sample-to-sample potential shifts in the analyte profiles, which are common in voltammetric studies. For tackling the first problem, it was necessary to correct the baselines of the recorded data. Concerning the second commented problem, some preprocessing alternatives were independently applied on the electrochemical responses. Voltammetric performance can be enhanced by eliminating noise and background components, thus baseline elimination is a crucial step for reducing both the complexity and the number of the unexpected components [53]. Considering this aim, we used the method proposed by Eilers et al. [54] for background elimination. No math will be described here; see Ref. [54] for all necessary equations and formalism. Moreover, it was demonstrated that the use of potential shift corrections improves the performance of resolution by second-order algorithms. Therefore, interest in potential shift correction continues. For correction of shifts or misalignments in data signals, a procedure termed COW was introduced by Nielsen et al. [55]. COW is a piecewise or segmented data preprocessing method aimed at justifying a sample data vector toward a reference vector by allowing limited changes in segments lengths on the sample vector. The ratio between the number of points in the reference vector N and the selected segment length I determines the number of segments, or rather the number of segment borders. An equal number of segments are specified on the sample vector. The maximum length increase or decrease in a sample segment is controlled by the so-called slack parameter t. In COW, the different segment lengths on the sample vector are selected (or the borders are shifted; "warped") so as to optimize the overall correlation between sample and reference. The problem is resolved by breaking down the global problem in a segment-wise correlation optimization by means of a dynamic programming algorithm (DP) [56,57]. The solution space of this optimization is described by two parameters: the number of segment borders $I+1$ and the length of the slack area t. It is usual to fix the initial and final boundaries so that the first and last points in the sample and reference vectors are forced to match. The algorithm is described in detail in the original papers [56,58–60].

2.1.4. Analytical figures of merit

Analytical figures of merit (AFOM), such as accuracy, sensitivity and selectivity, is an important necessity for the validation of chemometric methods. In chemometrics, the root mean squares error of prediction (RMSEP) generally expresses the accuracy of the model. It reports the closeness of agreement between the reference value and the value found by the model:

$$\mathrm{RMSEP} = \sqrt{\frac{\sum_{n=1}^{I}(y_{\mathrm{nominal}} - y_{\mathrm{predicted}})}{I-1}} \tag{5}$$

When expressing AFOM for multi-variate calibration methods, the part of the signal that relates uniquely to the analyte of interest is more important than the total signal. This unique signal is termed net analyte signal (NAS). For second-order data, the estimation of NAS is analogous to those for first-order procedures. In the present work, the NAS is the pure analyte data obtained by the second-order algorithms and can be calculated according to the following equation;

$$NAS_{ij} = a_{ij}(b_j \otimes c_j^T) \tag{6}$$

where NASij is the net analyte signal for the ith sample and jth analyte, a_{ij} is the obtained score, b_j and c_j are the loading vectors for other dimensions and $\otimes$ means the kronecker product. When using second-order advantage, each ith sample will have a specific value of NAS, and sensitivity (SENi) is estimated as the NAS at unit concentration, as shown in Eq. (7). Selectivity (SELi) is estimated as the ratio between SENi and the total signal, according to Eq. (8).

$$SEN_i = \|NAS_i\|_F \tag{7}$$

$$SEL_i = \frac{\|NAS_i\|_F}{\|N_i\|_F} \tag{8}$$

where N_i is the matrix of the total signal and the symbol $\|\ \|_F$ means the Frobenius norm of a matrix. A more in formative AFOM is the analytical sensitivity (γ), which is defined, as the ratio between SENi and the variance of instrumental signal, which may be estimated by replicate blank measurements:

$$\gamma_i = \frac{SEN_i}{S(0)} \tag{9}$$

The inverse of this parameter (γ^{-1}) reports the minimum concentration difference between two samples that can be determined by the model. Finally, according to Eq. (10) the limit of detection (LOD) can be estimated as 3.3 times the standard deviation for a sample of low or zero analyte concentration.

$$\mathrm{LOD} = 3.3S(0) \tag{10}$$

As the second-order advantage was applied, SEN and SEL determinations are sample specific and cannot be defined for the

multi-way method as a whole. In such cases, average values for a set of samples can be estimated and reported.

2.2. Experimental details

2.2.1. Chemicals and solutions

AC (Fluka), UA (Merck), FA (Sigma) and NE (Sigma) were used as received. All other chemicals (Merck) used were of analytical grade. A phosphate buffer solution (PBS, 0.1 mol L^{-1}) of pH 3.0 was prepared using Na_2HPO_4 and NaH_2PO_4. Stock solutions of UA (0.01 mol L^{-1}), AC (0.01 mol L^{-1}), NE (0.01 mol L^{-1}) and FA (0.01 mol L^{-1}) were prepared in PBS (0.1 mol L^{-1}, pH 3.0) and maintained in a refrigerator at 4 °C in dark (in these conditions they were stable for at least three months). From these solutions, working solutions were freshly prepared by taking appropriate aliquots and diluting with PBS to the desired concentrations. $[Fe(CN)_6]^{3-/4-}$ solution (redox probe, 5.0×10^{-3} mol L^{-1}) was prepared in PBS (0.1 mol L^{-1}, pH 3.0) and used for the measurements. All solutions were prepared with ultrapure water (UPW). The UPW was obtained from a Milli-Q water purification system from Millipore (provided by Kermanshah Oil Refining Company).

2.2.2. Apparatus and softwares

Electrochemical experiments were performed using a μ-AutolabIII/FRA2 controlled by the Nova software (Version 1.8). A conventional three-electrode cell was used with a saturated calomel electrode (SCE) as reference electrode, a Pt wire as counter electrode and a bare or modified GCE as working electrode. Electrochemical impedance spectroscopy (EIS) was carried out using the same three-electrode configuration above on the mentioned μ-Autolab in the PBS (0.1 mol L^{-1}, pH 3.0) and containing equimolar $[Fe(CN)_6]^{-4/-3}$ in a frequency range from 0.1 Hz to 100 kHz. A JENWAY-3345pH-meter equipped with a combined glass electrode was used to pH measurements. All the recorded electrochemical data was smoothed, when necessary, and converted to data matrices by the use of several home-made mfiles in MATLAB environment (Version 7.14, MathWorks, Inc.). Baseline correction routines based on an adaptation of the method described in Eilers et al. [54]. Data alignment using COW was performed in MATLAB environment. All the second-order algorithms used in this study were run in MATLAB environment. All the computations were performed on a DELL XPS laptop (L502X) with Intel Core i7-2630QM 2.0 GHz, 8 GB of RAM and Windows 7-64 as its operating system.

2.2.3. Electrode preparation

Prior to electrooxidation process, GCE was pretreated by mechanical and electrochemical polishing according to the following procedure. Before its first use the electrode surface was briefly scoured by a silicon carbide emery paper of 1200.0 grit to obtain a fresh surface. To smoothen the resulting relatively rough surface it was further subjected to sequential polishing by polishing cloth covered with alumina powder of 1.0, 0.3 and 0.05 mm particle size (Buehler, USA) for respectively 5.0, 10.0 and 20.0 min. To remove any adherent Al_2O_3 particles the electrode surface was rinsed thoroughly with UPW and cleaned in an ultrasonic bath containing UPW for 2.0 min. Further the GCE was oxidized by performing 10.0 cycles in 0.1 mol L^{-1} H_2SO_4 between 0.0 and 2.0 V at 0.1 V s^{-1}. The oxidized GCE was washed with UPW and transferred to pH 3.0 PBS for the further studies.

2.2.4. Preparation of real samples

A serum sample kindly provided by a Medical Diagnostic Laboratory in Kermanshah, Iran, was pretreated by the following procedure: to eliminate protein and other substances, 5.0 mL of human serum sample was placed in a10.0 mL glass tube and 5.0 mL of 15.0% (w/v) zinc sulfate solution-acetonitrile (50/40,v/v) was added. The glass tube was vortexed for 20.0 min, maintained at 4.0 °C for 15.0 min followed by centrifugation at 4000.0 rpm for 5.0 min. Then, the supernatant was collected in the same tube and this solution was used for subsequent analyses. Serum samples were partially diluted with PBS (0.1 mol L^{-1}, pH 3.0) and spiked with different amounts of AC, NE, UA, and or FA. Then, aliquots of the diluted samples were introduced into the electrochemical cell.

3. Results and discussion

3.1. Electrochemical studies

3.1.1. Characterization of OGCE

Fig. 1A shows the oxidation process of GCE. Here, the increasing anodic peak current indicates the oxidation process of GCE surface. To confirm the oxidized surface, it was transferred to PBS (0.1 mol L^{-1}, pH 3.0) for cyclic voltammetric (CV) studies. In PBS (0.1 mol L^{-1}, pH 3.0), the OGCE displays a couple of well-defined and reversible redox peak (Fig. 1B, curve *a*). At the same time, well-polished bare GCE (Fig. 1B, curve *b*) fails to exhibit such kind of redox peak in PBS (0.1 mol L^{-1}, pH 3.0). This examination validates the oxidized surface of GCE. The electrochemical oxidation process of GCE results in the formation of functional groups like carbonyl, quinoid, carboxyl and hydroxyl radical species on the electrode surface [60]. In particular, the formation of these functional groups exhibits a redox peak and gives the special electrochemical properties. Further based on the previous literature reports [60–63] it was found that the important oxygen functional group found on the electrode surface supposed to be carboxyl and the remaining is carbonyl, etc. At the same time, we did not mean that other groups (carbonyl, quinoid and hydroxyl) did not involve in electrocatalytic process, but we are assuming that carboxyl group will be the major functional group for the proposed electrode. Further, [60–62,64] clearly report about the surface porous nature of GCE. They have claimed that anodic pretreatment process does not create any porous nature but opens the closed pores which already present on electrode surface [60,65]. Thus, this type of oxidation will result in the formation of porous nature on electrode surface [60]. Further the OGCE was examined for different scan rate studies in PBS (0.1 mol L^{-1}, pH 3.0). Fig. 1C exhibits the CVs of the OGCE in PBS (0.1 mol L^{-1}, pH 3.0) at different scan rates in the range of 0.01–1 V s^{-1}. Here, by increasing the scan rate, both peak currents increase and oxidation and reduction peaks shift to more and less potentials, respectively. Also, the anodic and cathodic peak currents were linearly dependent on the scan rate (Fig. 1D), which indicates that OGCE surface reaction was a surface-controlled process. The Nyquist plot of EIS of OGCE (Fig. 1E, curve *a*) is smaller compared with GCE (curve *b*) it indicates that the surface of OGCE has been modified with the functional groups which make the electron transfer kinetics process as a faster one, because electrochemical oxidation of GCE increases porosity of GCE and improves electron transfer kinetic between analyte and electrode. Furthermore, the OGCE has been examined in various pH solutions (not shown). From the plot of formal potentials ($E^{0\prime}$) vs. pH of the OGCE, the slope value was found as 54 mV/pH, which is close to the expected value of 59 mV/pH for one electron and one proton reaction process, respectively.

The surface areas of GCE, and OGCE were evaluated by the Randles–Sevcik equation (298.15 K), using the redox currents of the ferricyanide (i_p):

$$i_p = (2.678\times10^5)n^{3/2}\,\upsilon^{1/2}\,D^{1/2}\,AC \qquad (11)$$

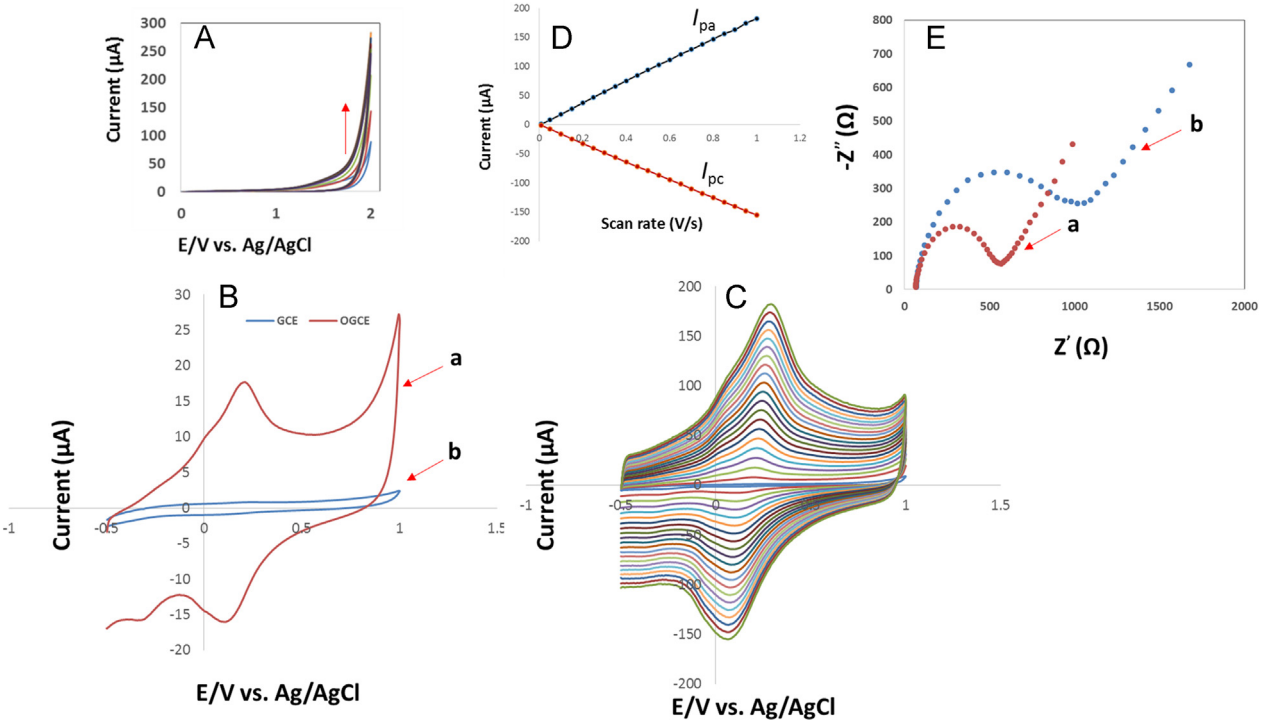

Fig. 1. (A) Electrooxidation process of GCE in 0.1 mol L^{-1} H_2SO_4 in the range of 0.0 and 2.0 V for 10.0 cycles at 0.05 V s^{-1}. (B) CV response of (a) OGCE and (b) bare GCE in PBS (0.1 mol L^{-1}, pH 3.0). (C) CV response of OGCE in PBS (0.1 mol L^{-1}, pH 3.0) at different scan rates: 0.01–1.0 V s^{-1}. (D) The plot of cathodic and anodic peak currents of OGCE vs. scan rate. (E) EIS curves of (a) OGCE and (b) bare GCE in PBS (0.1 mol L^{-1}, pH 3.0).

where *D*, the diffusion coefficient of the ferricyanide, was 6.3×10^{-6} cm^2 s^{-1}; *n* and *C* represent the transferring electron number and the concentration (mol dm^{-3}) of the ferricyanide; *υ* was the scan rate (V s^{-1}); and *A* was the surface area (cm^2). The surface area of the bare GCE is calculated to be 0.124 cm^2. After oxidation of GCE, the redox current of the ferricyanide enlarged about 23%, indicating that the OGCE has an apparent surface area of 0.152 cm^2. From these results, it can be confirmed that the formation of oxygen functional groups did enhance the electron transfer between the analyte and the electrode interface.

Stability of the OGCE was investigated by storing at room temperature in presence and absence of pH 3.0 PBS. It was stable for 4.0 weeks and after 4.0 weeks a gradual decrease (8%) has been found from the current initial values. The OGCE can be prepared within 12.0 min and by manual polishing with alumina slurry we can retain the original nature of the GCE very easily. The background current variations of the OGCE surface at five GCE were less than 5.0% which validates the reproducible nature of the oxidized effect on the GCE surface. These results suggest that the OGCE possesses the long term stability and reproducibility.

3.1.2. Voltammetric characteristics of AC, NE, UA, and FA at OGCE

Effect of solution pH on electrochemical response of OGCE toward simultaneous determination of AC, NE, and UA was studied using CV. Fig. 2A–C shows the influence of pH of the PBS, in the range of 2.0–12.0, on the signal intensities of AC, NE, and UA, respectively. As can be observed in Fig. 2, all anodic peak currents of the studied analytes have a maximum value at pH 3.0. Taking into account that for analytical purposes both maximal and stable currents are necessary, a pH value of 3.0 was selected for further experiments.

The effect of scan rate on the electrocatalytic oxidation of AC, NE, and UA at the OGCE was investigated by CV (not shown). Plots of anodic peak current versus the square root of scan rate in the range of 10–500 mV s^{-1}, was constructed (not shown). These plots were found to be linear, suggesting that the processes were diffusion-controlled.

The individual electrocatalytic oxidation of AC, NE, and UA at GCE (Fig. 3A) and OGCE (Fig. 3B) was investigated using CV. Here, the OGCE reduces the anodic over potentials and increases anodic peak currents of AC and NE, but increases both anodic over potential and anodic peak current of UA comparing with GCE. The next attempt was employed for the simultaneous determination of AC, NE, and UA. The oxidation peak potential for FA (Fig. 3B, curve *d*) is very close to those of AC (curve *a*) and UA (curve *c*). Consequently, FA is one of the usual interferences in the determination of AC, NE, and UA. Therefore, interest in exploiting second-order advantage from voltammetric data for the simultaneous determination of AC, NE, and UA in the presence of FA continues.

3.2. Chemometric studies

3.2.1. Calibration, validation, and test sets

Since DPV has a much higher current sensitivity than CV, it has been used to simultaneous determination of the studied analytes. Prior to the second-order calibration experiment, a calibration graph (not shown) has been constructed for each analyte of interest, by varying the concentration values and registering voltammograms at the optimised conditions in DPV. Univariate calibrations indicated that, under the established working conditions (PBS 0.1 mol L^{-1}, pH 3.0 and DPV conditions: step potential 0.025 V, pulse height 0.05 V, pulse time 0.05 s, and scan rate 0.05 V s^{-1}), linearity is held in the range 1.0 to 4400.0×10^{-6} mol L^{-1}, 0.1 to 43.9×10^{-6} mol L^{-1}, and 20.0 to 481.0×10^{-6} mol L^{-1} for AC, NE, and UA, respectively, which were the limiting assayed concentrations in subsequent analyzes.

A calibration set of 14 samples containing AC, NE, and UA was prepared in PBS (0.1 mol L^{-1}, pH 3.0) according to a central composite design (Table 1). A validation set of 10 synthetic mixtures containing only AC, NE, and UA was prepared in PBS (0.1 mol L^{-1}, pH 3.0) with random concentrations in the ranges defined by the univariate calibrations (Table 1). A test set of 10 synthetic mixtures

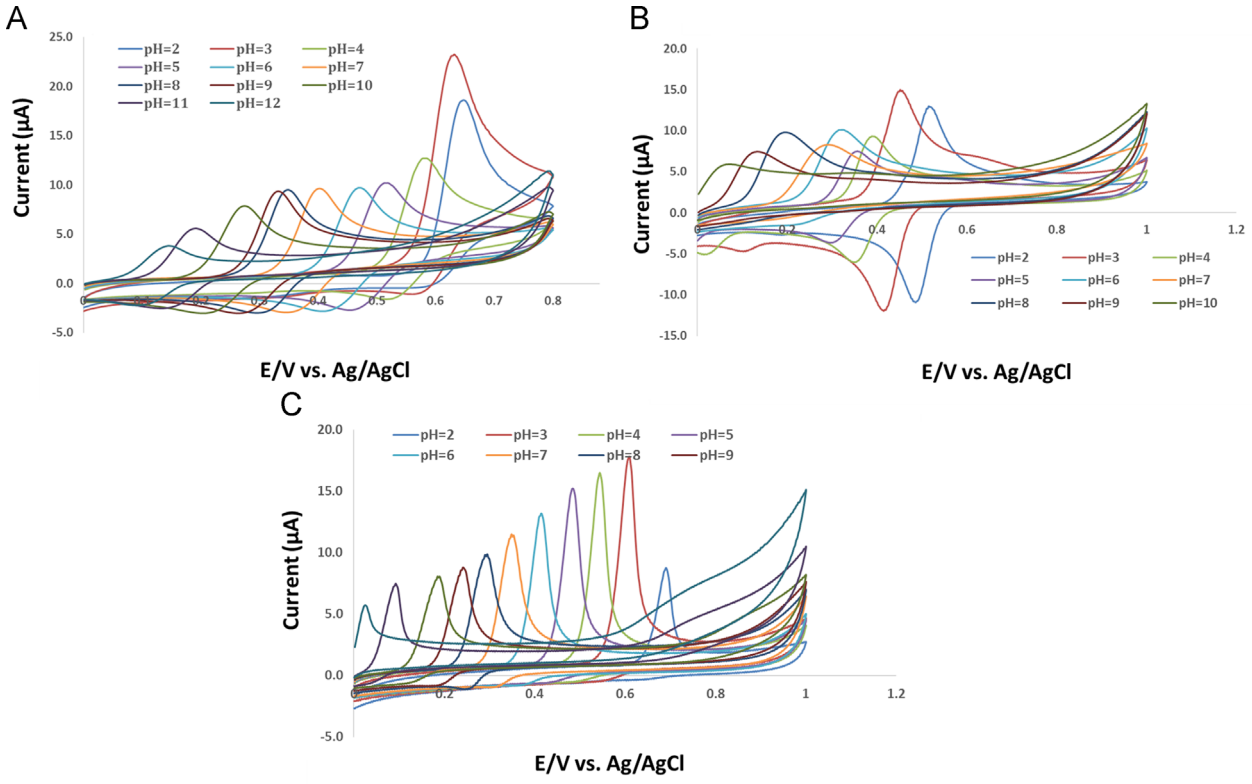

Fig. 2. Cyclic voltammograms of (A) AC (1.0×10^{-3} mol L^{-1}), (B) NE (1.0×10^{-3} mol L^{-1}), and (C) UA (1.0×10^{-3} mol L^{-1}) in PBS (0.1 mol L^{-1}) at OGCE at different pHs.

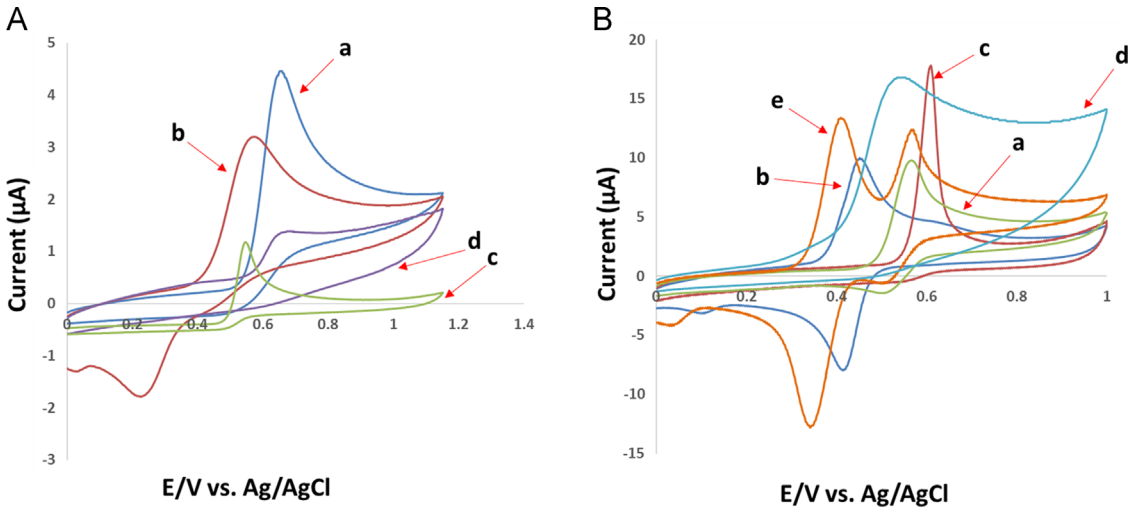

Fig. 3. (A) Cyclic voltammograms of (a) AC (1.0×10^{-3} mol L^{-1}), (b) NE (1.0×10^{-3} mol L^{-1}), (c) UA (1.0×10^{-3} mol L^{-1}), and (d) FA (1.0×10^{-3} mol L^{-1}) at GCE in PBS (0.1 mol L^{-1}, pH 3.0), and (B) cyclic voltammograms of (a) AC (1.0×10^{-3} mol L^{-1}), (b) NE (1.0×10^{-3} mol L^{-1}), (c) UA (1.0×10^{-3} mol L^{-1}), (d) FA (1.0×10^{-3} mol L^{-1}), and mixture of AC, NE, and UA at OGCE in PBS (0.1 mol L^{-1}, pH 3.0). In all cases scan rate is 0.05 V s^{-1}.

containing random concentrations of AC, NE, and UA was prepared in PBS (0.1 mol L^{-1}, pH 3.0) to which FA was added as uncalibrated interference (Table 1). For all calibration, validation, and test sets, DPVs of the each mixture of were recorded in different pulse heights of 0.015–0.09 V with a 0.015 V interval.

3.2.2. *U-PLS/RBL and N-PLS/RBL applied to the second-order data*

Appling chemometrics tools such as U-PLS/RBL and N-PLS/RBL to resolve data requires the uniform presentation of data, i.e., all signals have to be adjusted to the same length and corresponding variables have to be placed into the proper columns of the data matrix. The signals obtained from voltammetric techniques often do not fulfill this requirement. This problem is seen as the potential shift in electrochemical data. These facts cause a decrease in the linearity, which depends on the magnitude of the potential shift. A number of algorithms is available for performing data alignment and one of the most flexible ones in this regard is COW. Potential shift- and baseline corrections were performed on a column-wise augmented data matrix containing the raw data (Fig. 4A–C) related to calibration or validation or test set. Fig. 4D–F shows the results of applying COW for data alignment and it confirms the capability of COW for aligning the

Table 1
Composition of the samples used in the calibration, validation, and test sets.

Sample	Calibration (10^{-6} mol L^{-1})			Sample	Validation (10^{-6} mol L^{-1})			Sample	Test (10^{-6} mol L^{-1})			
	AC	NE	UA		AC	NE	UA		AC	NE	UA	FA
1	734.6	29.2146	76.987	1	56	5	78	1	5	5	25	45
2	2934.1	7.3146	76.987	2	345	9	35	2	15	34	45	130
3	2199.5	21.9	20	3	780	12	160	3	260	40	56	75
4	2199.5	0.1	230.5	4	1200	28	110	4	650	28	75	450
5	1	21.9	230.5	5	45	6	35	5	3800	16	440	20
6	4400	0.1	20	6	300	33	57	6	4200	18	65	240
7	1	0.1	481	7	245	38	48	7	120	28	32	390
8	1464.9	14.5854	153.513	8	0	21	220	8	70	32	140	32
9	4400	0.1	481	9	1800	0	340	9	35	35	180	15
10	1	43.9	20	10	110	7	0	10	90	10	74	98
11	734.6	7.3146	307.487	–	–	–	–	–	–	–	–	–
12	4400	0.1	20	–	–	–	–	–	–	–	–	–
13	1	43.9	20	–	–	–	–	–	–	–	–	–
14	2199.5	21.9	20	–	–	–	–	–	–	–	–	–

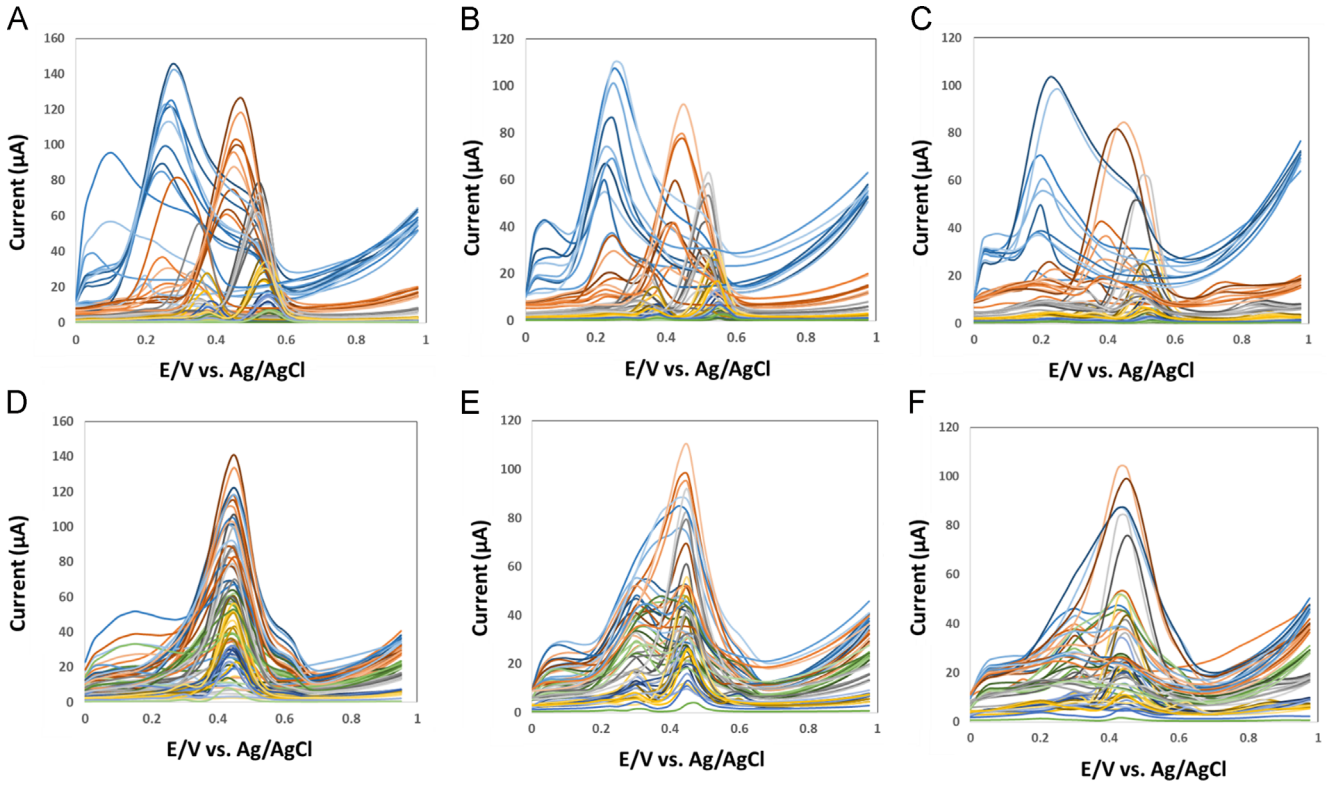

Fig. 4. (A) Raw voltammograms of the calibration set, (B) raw voltammograms of the validation set, (C) raw voltammograms of the test set, (D) pretreated data (potential shift- and baseline corrected data) of the calibration set, (E) pretreated data (potential shift- and baseline corrected data) of the validation set, and (F) pretreated data (potential shift- and baseline corrected data) of the test set.

data. Significant changes in baselines were then eliminated by the method proposed by Eilers et al. [54], Fig. 4D–F. The pre-treated data (potential shift- and baseline corrected data) was then used for next computations.

In U-PLS/RBL and N-PLS/RBL, the selection was performed using the cross-validation method described by Haaland and Thomas [66,67] over just the calibration set. The optimum number of factors is estimated by calculating the ratio $F(A)=\mathrm{PRESS}(A<A*)/\mathrm{PRESS}(A)$, where PRESS is the predicted error sum of squares, defined as $\mathrm{PRESS}=\Sigma(y_{\mathrm{nominal}}-y_{\mathrm{predicted}})^2$, A is a trial number of factors and $A*$ corresponds to the minimum PRESS. The number of optimum factors was selected as that leading to a probability of less than 75% and $F>1$. Note that RBL is not required for calibration samples because they did not include unexpected components. The results of cross-validation to determine the number of latent variables for U-PLS and N-PLS are summarized in Table 2. This analysis led to the conclusion that the latter number is 3 for the most cases, as expected for this system using a mean centering procedure, with the exception of the 4 value for NE processed with N-PLS. The presence of non-linearities which are usually found in electrochemical data causes more latent variables to model the variability of the data but in the present study this limitation was tackled by potential shift correction.

When unexpected components take place in the samples, the RBL procedure is then applied to the unfolded validation or test data and the outcome scores are free from interferents signal,

Table 2
Cross-validation results for calibration samples using U-PLS and N-PLS.

AC				NE				UA			
U-PLS	PRESS	F	P	**U-PLS**	PRESS	F	P	**U-PLS**	PRESS	F	P
1	8.8×10^{5}	95.9	0.998	1	6.7×10^{5}	95.3	0.998	1	9.1×10^{5}	75.6	0.999
2	6.4×10^{4}	6.3	0.996	2	3.8×10^{4}	5.4	0.997	2	4.6×10^{4}	5.3	0.998
3	$\mathbf{8.8\times10^{3}}$	**1.2**	**0.554**	**3**	$\mathbf{7.1\times10^{3}}$	**1.1**	**0.598**	**3**	$\mathbf{7.5\times10^{3}}$	**1.1**	**0.654**
4	7.9×10^{3}	1.0	0.453	4	6.9×10^{3}	1.0	0.497	4	7.6×10^{3}	1.0	0.532
5	8.1×10^{3}	–	–	5	6.8×10^{3}	–	–	5	7.5×10^{3}	–	–
6	7.6×10^{3}	–	–	6	6.7×10^{3}	–	–	6	7.3×10^{3}	–	–
7	7.5×10^{3}	–	–	7	6.5×10^{3}	–	–	7	7.2×10^{3}	–	–
8	7.6×10^{3}	–	–	8	6.5×10^{3}	–	–	8	7.4×10^{3}	–	–
N-PLS				**N-PLS**				**N-PLS**			
1	7.8×10^{5}	95.2	0.998	1	7.6×10^{6}	96.2	0.998	1	6.1×10^{5}	75.3	0.998
2	8.0×10^{4}	5.4	0.997	2	4.0×10^{5}	88.3	0.989	2	5.4×10^{4}	6.1	0.991
3	$\mathbf{6.8\times10^{3}}$	**1.1**	**0.588**	3	4.3×10^{4}	6.6	0.978	**3**	$\mathbf{6.5\times10^{3}}$	**1.2**	**0.554**
4	6.6×10^{3}	1.0	0.476	4	5.9×10^{3}	**1.2**	**0.612**	4	6.6×10^{3}	1.0	0.431
5	6.5×10^{3}	–	–-	5	5.8×10^{3}	1.0	0.513	5	6.5×10^{3}	–	–
6	6.5×10^{3}	–	–	6	5.6×10^{3}	–	–	6	6.3×10^{3}	–	–
7	6.4×10^{3}	–	–	7	5.5×10^{3}	–	–	7	6.2×10^{3}	–	–
8	6.4×10^{3}	–	–	8	5.5×10^{3}	–	–	8	6.4×10^{3}	-	–

providing the so-called second-order advantage to the methodology. Therefore, the next step was to estimate the number of unexpected components in validation and test samples via the post-calibration RBL procedure. This was done by considering the variation of the residual as a function of the trial number of unexpected components. The stabilization of the residual around the instrumental noise ($\sim 2\times10^{-7}$) suggested one unexpected component. Using suitable latent variables described in Table 2 for modeling the calibration data and a single unexpected component for RBL, the U-PLS/RBL and N-PLS/RBL were applied to the validation and test samples. The good agreement that exists among the predicted and the nominal concentrations of the analytes (see Table 3) demonstrates the success of RBL in extracting the spectral contributions of the unknown component from the sample. This ability, which refers to the second-order advantage with U-PLS/RBL and N-PLS/RBL algorithms, makes prediction possible with no potential interference from the sample.

3.2.3. *ANN-RBL applied to the second-order data*

Intrinsically non-linear data cannot be processed with classical calibration methods resorting to linear underlying models. It is possible that in the above mentioned cases one may find local variable regions where the response behavior towards analyte concentrations is approximately linear. However, if the whole set of instrumental data needs to be explored, one has to resort to alternatives which include, for example, ANNs. The back-propagation of errors method was selected for training the ANNs. Unfolded principal component analysis (U-PCA/RBL) is a recent model, developed to obtain the second-order advantage from non-linear second-order signals. The baseline corrected data without any shift correction was decomposed by U-PCA/RBL to obtain scores for training and prediction by back-propagation ANN. The average training parameters for the three experimental data sets herein studied are collected in Table 4. Results of application of ANN/RBL to validation and test sets are shown in Table 3.

3.2.4. *MCR-ALS and PARAFAC2 applied to the second-order data*

The main premise of multivariate curve resolution (MCR) techniques is to follow the multicomponent Beer's law. Consequently, they can be used to analyze the bilinear data. Appling chemometrics tools such as MCR-ALS to resolve data requires the uniform presentation of data, i.e., all signals have to be adjusted to the same length and corresponding variables have to be placed into the proper columns of the data matrix. The signals obtained from voltammetric techniques often do not fulfill this requirement. This problem is seen as the potential shift in electrochemical data. These facts cause a decrease in the linearity, which depends on the magnitude of the potential shift. In many cases, large lof values as the results of potential shift for MCR-ALS analysis are obtained and impel the analyst to use a higher number of components to explain the non-linearity.

MCR-ALS as a powerful chemometrical method was applied on a column-wise augmented data matrix (the calibration matrices and the unknown matrix are placed adjacent to each other), because this permits differentiation between the analyte and the interferents. This algorithm needs initialization with system parameters as close as possible to the final results. Therefore, analyte and interference voltammograms are required owing that the resolution is based on the selectivity in the latter mode. In this work, the selection of the purest voltammogram for the interferent was made based using homemade routines based on SIMPLISMA (simple interactive self-modeling mixture analysis) [68]. The number of contributing species in the system under study when applying singular value decomposition (SVD) was always equal to the real number of components, i.e. four when analyzing test samples.

The applied constraints in ALS were non-negativity, and unimodality (for voltammogram profiles). The lack of linearity in the system produced large excessive lack of fit (lof) values (all larger than 20%) and convergence was not achieved and the results of MCR-ALS were not satisfactory. The inefficiency of the MCR-ALS model could be due to the potential shift of the data. The shift of potential in the data as a possible source of inefficiency was therefore corrected. Although the potential shift correction can overcome the non-bilinearity in the data, it produces rank deficient data. We therefore tried to overcome the rank deficiency problem using matrix augmentation. The potential shift corrected data were then augmented and standard MCR-ALS was performed on the new augmented data. Applying MCR-ALS on the augmented potential shift corrected data produced a low lof value (all smaller than 7%) which was better than that obtained without the potential shift correction. The results of applying MCR-ALS on potential shift corrected data for the determination of the analytes of interest in validation or test data sets are given in Table 3.

Table 3
Predicted and nominal concentrations (10^{-6} mol L^{-1}) of the studied analytes in validation and test sets by the second-order algorithms.

AC	Predicted					NE	Predicted				UA	Predicted				
Nominal	**U-PLS/RBL**	**ANN/RBL**	**N-PLS/RBL**	**MCR-ALS**	**PARAFAC2**	**Nominal**	**U-PLS/RBL**	**ANN/RBL**	**N-PLS/RBL**	**MCR-ALS**	**PARAFAC2**	**Nominal**	**U-PLS/RBL**	**ANN/RBL**	**N-PLS/RBL**	**MCR-ALS**	**PARAFAC2**
Validation set																	
56	55	54.7	54	53	52	5	4.9	5.1	4.9	5.3	5.5	78	78	77.6	77	79	80
345	344	346.2	342	340	342	9	9.1	8.9	8.8	9.4	9.8	35	35.3	34.5	34.2	36	36.4
780	779	778.9	777	785	787	12	12	12.05	11.9	12.2	12.4	160	161	159.6	159	161.3	162
1200	1199	1201.2	1198	1206	1208	28	28.05	28.1	27.6	28.4	28.6	110	110	109.8	109	111	112
45	44.3	46	44	47	49	6	6.01	6.08	5.9	6.2	6.3	35	34.8	34.6	34	36	36.8
300	299	298.7	298	304	306	33	32.9	32.9	32.8	33.6	33.8	57	56.3	56.2	56	59	59.5
245	244	243.8	243	248	252	38	37.9	37.6	37.8	38.6	38.9	48	49	47.5	47	46	45
0	0.007	0.01	0.01	0.1	0.13	21	20.9	20.9	20.7	21.6	21.8	220	221	219	218	217	216
1800	1804	1806	1811	1819	1821	0	0.01	0.01	0.02	0.05	0.06	340	339	338.5	338	337	336
110	110	109.3	109	113	111	7	7.05	6.96	6.9	7.3	7.6	0	0.001	0.01	0.02	0.04	0.05
Test set																	
5	4.9	4.8	4.6	4.5	4.4	5	5.05	5.1	5.2	5.3	5.4	25	24.7	23.6	23.4	23	22.8
15	15.1	15.3	15.5	15.7	15.9	34	33.8	35	35.6	36	37	45	45.3	46	46.1	46	47
260	259	262	263	264	265	40	40.2	41	41.3	41.5	41.8	56	56.5	57	57.3	57.6	58
650	648	653	654	655	656	28	27.8	29	29.4	29.7	29.9	75	75.6	76	74.5	74	73
3800	3789	3814	3783	3780	3778	16	16.1	15.1	15	14.8	14.6	440	440.3	442	438.3	438	437
4200	4207	4210	4213	4214	4216	18	18.1	18.8	18.9	19	19.3	65	65.4	66	64	63	62.6
120	119	122	124	125	126	28	27.8	28.7	28.8	29	29.5	32	32.3	33	33.5	33	33.4
70	71	72	73	74	75	32	32.3	33	33.2	33	33.5	140	140.9	138	142	143	144
35	36	37	33.3	37	38	35	35.3	36	36.2	36.4	37	180	180.3	178	183	184	175
90	91	93	93.4	94	85	10	10.2	10.6	10.7	10.9	11	74	74.5	72	71	70.6	70

Table 4
ANN training results for all data sets.

	Value
AC	
Architecture (input-hidden-output neurons)	5–8–1
Number of training epoch	583–1075
Learning rate	0.5
Momentum	0.5
NE	
Architecture (input-hidden-output neurons)	3–6–1
Number of training epoch	1114–11234
Learning rate	0.5
Momentum	0.5
UA	
Architecture (input-hidden-output neurons)	3–8–1
Number of training epoch	745–8354
Learning rate	0.5
Momentum	0.5

PARAFAC2 as an advanced and more flexible variant of the PARAFAC algorithm was developed to manipulate the three-way data types deviated from trilinearity conditions [69–71]. Non-trilinear data structure can be faced when retention time shifts or shape changes of profiles from sample to sample happens. PARAFAC2 model for each slab of third-order tensor X can be defined as follows:

$$X_k = AD_k(B_k)^{\mathrm{T}} + E_k \quad k = 1, \ldots, K \tag{12}$$

where in chromatographic systems, $X_k(I \times J)$ represents the chromatographic data related to the kth run. K is the number of runs or samples. $A_k(I \times F)$ is the loading matrix of first mode (resolved voltammograms of F analytes), $D_k(\mathrm{F} \times \mathrm{F})$ is a diagonal matrix holding the kth row of the sample-mode loading matrix C, $B_k(J \times F)$ is the kth profiles of the second mode and E_k is the matrix of residuals. The initial estimates for the model has been obtained using singular value decomposition (SVD) and the data analysis has been performed with non-negativity constraints in the first and third dimensions. As convergence criterion an absolute change of 1×10^{-7} has been used in percent variance explained. More details about the model and algorithm are in the literature [69].

A three-way array, X was obtained by stacking K calibration standards and one validation or test sample ($K+1$ runs). Then individual PARAFAC2 models were built each time by including one of the validation or test samples in the array. Proper number of factors was selected. In this work, the correct number of factors for each sample was determined by calculating the explained variance of the model. Results of application of PARAFAC2 to validation and test sets are shown in Table 3.

3.2.5. *Comparison of predictive ability of the second-order algorithms*

In order to comparison of predictive ability of the second-order algorithms, the predicted concentrations of both validation and test sets (Table 3) were regressed on the nominal concentrations (not shown). In this case an ordinary least squares (OLS) analysis of predicted concentrations versus nominal concentrations was applied [72]. The calculated intercept and slope were compared with their theoretically expected values (intercept=0, slope=1), based on the elliptical joint confidence region (EJCR) test. If the ellipses contain the values 0 and 1 for intercept and slope (ideal point), respectively, showing the predicted and nominal values do not present significant difference at the level of 95% confidence and the elliptic size denotes precision of the analytical method, smaller size corresponds to higher precision [73]. Fig. 5A – F shows

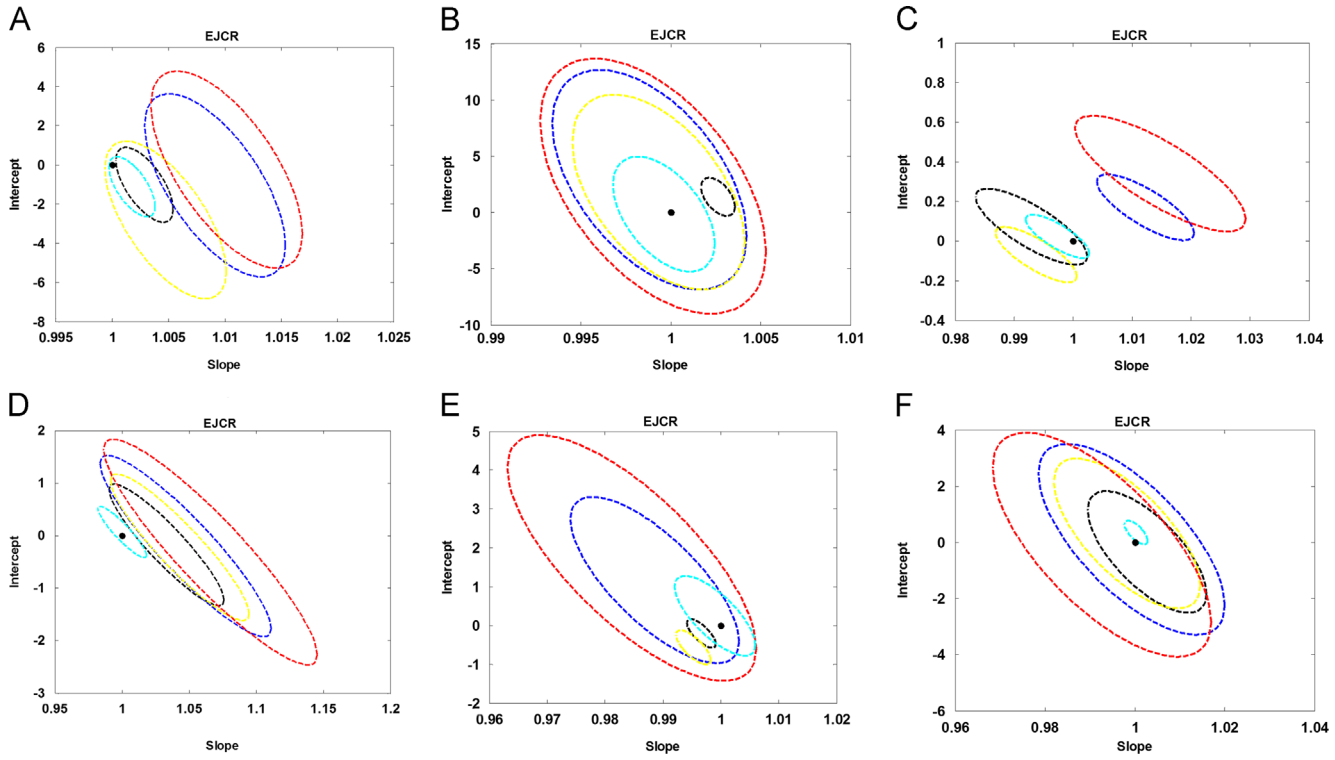

Fig. 5. Elliptical joint regions (at 95% confidence level) for the slopes and intercepts of the regressions for (A) AC, validation set, (B) AC, test set, (C) NE, validation set, (D) NE, test set, (E) UA, validation set, and (F) UA, test set. In all cases: black point marks the theoretical point (0,1), black ellipse shows ANN results, blue ellipse shows MCR-ALS results, yellow ellipse shows N-PLS/RBL results, red ellipse shows PARAFAC2 results, and cyan ellipse shows U-PLS/RBL results. (For interpretation of the references to color in this figure legend, the reader is referred to the web version of this article.)

Table 5
Analytical figures of merit for determination of AC, NE, and UA by U-PLS/RBL.

Analyte	SEN (μA $(10^{-6}$ mol $L^{-1})^{-1}$)	SEL	LOD (10^{-6} mol L^{-1})	RMSEP (10^{-6} mol L^{-1})	Analytical sensitivity $(10^{-6}$ mol $L^{-1})^{-1}$
Validation set					
AC	3.1	0.75		0.39	63.2
NE	2.9	0.71		0.32	51.8
UA	2.85	0.69		0.41	54.3
Test set					
AC	2.8	0.69		0.28	68.9
NE	2.85	0.72		0.36	55.4
UA	2.74	0.66		0.47	52.3

the corresponding ellipses of the EJCR analyses. As can be concluded from Fig. 5A–F, the best predictions for AC, NE, and UA in both validation and test sets were obtained by U-PLS/RBL (cyan ellipse) which shows the accurate determination of analytes by the developed methodology. If the EJCRs of U-PLS/RBL for UA determination in test set are analyzed (Fig. 5F), it is notable that the ideal point falls on the cyan ellipse, denoting slightly poorer prediction accuracy for UA in test set.

Analytical figures of merit (AFOM) for the proposed U-PLS/RBL method including sensitivity (SEN), analytical sensitivity (γ), selectivity (SEL), limit of detection (LOD) and RMSEP are summarized in Table 5. From Table 5, it can be seen that the U-PLS/RBL model offers a very sensitive and selective method for simultaneous determination of AC, NE, and UA.

3.2.6. *Analysis of human serum samples*

In view of the above results, U-PLS/RBL was selected as the algorithm to be applied to real samples. To evaluate the feasibility of the proposed method, simultaneous quantification of AC, NE, and UA in the presence of FA was performed in partially diluted human serum samples. Serum samples were partially diluted with PBS (0.1 mol L^{-1}, pH 3.0) and spiked with different amounts of AC, NE, UA, and FA. Then, aliquots of the diluted samples were introduced into the electrochemical cell. The DPV signals of the prepared samples in optimized conditions and different pulse heights (15 to 90 mV with 15 mV increment) at the OGCE were recorded. The recovery rates of the spiked samples were achieved between 97% and 105.88%, showing that the blood serum matrix does not show any significant interference in our analysis (Table 6).

4. Conclusion

This study describes a very attractive methodology for the simultaneous determination of AC, NE, and UA in the presence of FA at the surface of OGCE by recording three-way voltammetric arrays, and applying several second-order algorithms such as U-PLS/RBL, N-PLS/RBL, ANN-RBL, MCR-ALS and PARAFAC2. The main goals of this work were (i) to create electrochemical

Table 6
Results of simultaneous determination of AC, NE, and UA in human serum sample by U-PLS/RBL.

Sample	Added (10^{-6} mol L^{-1})				Found (10^{-6} mol L^{-1})			Recovery (%)		
	AC	**NE**	**UA**	**FA**	**AC**	**NE**	**UA**	**AC**	**NE**	**UA**
1	**None**	20	40	45	**N.D**[a]	19.4	43.5	-	97	105.88
2	30	**None**	250	87	31	**N.D**	255	103.2	–	101.9
3	150	11	**None**	**34**	147.3	11.3	**N.D**	98.2	100.9	–
4	210	28	135	20	216	28.6	137	102.8	102	101.45
5	60	10	85	60	58.2	10.2	83	97	101.96	97.65

[a] Not detected.

second-order data and (ii) to perform the analysis in the presence of an unexpected interference. To achieve the first goal, second-order data were created using a simple change in pulse height of DPVs. Because of the non-linear behavior of the recorded voltammetric data, the potential shift correction was performed. The use of three-way data, exploiting the information contained in full voltammetric matrices and second-order algorithms, allowed the successful simultaneous determination of AC, NE, and UA in both synthetic and real samples even in the presence of FA as an unexpected interference. Among the second-order algorithms analyzed, U-PLS/RBL showed the best results for determination of three analytes even in the presence of FA as an unexpected interference. This is the newest example of the power of U-PLS/RBL for processing of multi-way electrochemical data. The proposed methodology in this study exploited the second-order advantage and also demonstrated that combination of electrochemical measurements with U-PLS/RBL method turned possible the simultaneous determination of AC, NE, and UA in the presence of FA as uncalibrated interference in complex matrices such as human serum, despite the serious interference from the background components. The potential advantages of this determination, such as sensitivity, rapidity and low-cost, can be even more highlighted by considering the possibility of the proposed method for biosensing and clinical applications.

Acknowledgements

The authors wish to express their sincere appreciation to Razi University Research Council, the UNL, CONICET and ANPCyT for financial support of this project.

References

[1] R. Bro, Crit. Rev. Anal. Chem. 36 (2006) 279–293.
[2] G.M. Escandar, N.M. Faber, H.C. Goicoechea, A. Muñoz de la Peña, A.C. Olivieri, R.J. Poppi, Trends Anal. Chem. 26 (2007) 752–765.
[3] A.C. Olivieri, G.M. Escandar, A. Muñoz de la Peña, Trends Anal. Chem. 30 (2011) 607–617.
[4] K.S. Booksh, B.R. Kowalski, Anal. Chem. 66 (1994) 782–791.
[5] C.N. Ho, G.D. Christian, E.R. Davidson, Anal. Chem. 50 (1978) 1108–1113.
[6] A.C. Olivieri, Anal. Chem. 80 (2008) 5713–5720.
[7] D. Voet, J.G. Voet, Biochemistry, second ed., Wiley, New York, 1995.
[8] M.H. Sorouraddin, J.L. Manzoori, E. Kargarzadeh, A.M. Haji-Shabani, J. Pharm. Biomed. Anal. 18 (1998) 877–881.
[9] M. Novotny, V. Quaiserová-Mocko, E.A. Wehrwein, D.L. Kreulen, G.M. Swain, J. Neurosci. Methods 163 (2007) 52–59.
[10] O. Gyllenhaal, L. Johansson, J. Vessman, J. Chromatogr. A 190 (1980) 347–357.
[11] V. Carrera, E. Sabater, E. Vilanova, M.A. Sogorb, J. Chromatogr. B 847 (2007) 88–94.
[12] M. Mazloum-Ardakani, M.A. Sheikh-Mohseni, M. Abdollahi-Alibeik, A. Benvidi, Sens. Actuators, B 171-172 (2012) 380–386.
[13] R.N. Goyal, M. Abdul Aziz, M. Oyama, S. Chatterjee, A. Raj, S. Rana, Sens. Actuators, B 153 (2011) 232–238.
[14] G.R. Xu, H.Y. Chang, H. Cho, W. Meng, I.K. Kang, Z.U. Bae, Electrochim. Acta 49 (2004) 4069–4077.
[15] M. Mazloum-Ardakani, H. Beitollahi, M.K. Amini, F. Mirkhalaf, B.B.F. Mirjalili, Biosens. Bioelectron. 26 (2011) 2102–2106.
[16] F.F. Daly, J.S. Fountain, L. Murray, A. Graudins, N.A. Buckley, Med. J. Aust. 188 (2008) 296–301.
[17] A.M. Larson, J. Polson, R.J. Fontana, T.J. Davern, J.S. Reisch, F.V. Schiødt, G. Ostapowicz, A.O. Shakil, W.M. Lee, Hepatology 42 (2005) 1364–1372.
[18] J.T. Afshari, T.Z. Liu, Anal. Chim. Acta 443 (2001) 165–169.
[19] M.A. Campanero, B. Calahorra, E. Garcia-Quétglas, A. López-Ocáriz, J. Honorato, J. Pharm. Biomed. Anal. 20 (1999) 327–334.
[20] F. Ghorbani-Bidkorbeh, S. Shahrokhian, A. Mohammadi, R. Dinarvand, Electrochim. Acta 55 (2010) 2752–2759.
[21] C.X. Xu, K.J. Huang, Y. Fan, Z.W. Wu, J. Li, J. Mol. Liq. 165 (2012) 32–37.
[22] R.N. Goyal, V.K. Gupta, S. Chatterjee, Sens. Actuators, B 149 (2010) 252–258.
[23] R.N. Goyal, V.K. Gupta, M. Oyama, N. Bachheti, Electrochem. Commun. 7 (2005) 803–807.
[24] V.K. Gupta, R. Jain, K. Radhapyari, N. Jadon, S. Agarwal, Anal. Biochem. 408 (2011) 179–196.
[25] P. Kalimuthu, S. Abraham John, Anal. Chim. Acta 647 (2009) 97–103.
[26] H. Beitollahi, I. Sheikhshoaie, Anal. Methods 3 (2011) 1810–1814.
[27] J. Ping, J. Wu, Y. Wang, Y. Ying, Biosens. Bioelectron. 34 (2012) 70–76.
[28] H. Beitollahi, A. Mohadesi, S. Khalilizadeh Mahani, A. Akbari, Anal. Methods 4 (2012) 1029–1035.
[29] S. Daya, S. Anoopkumar-Dukie, Life Sci. 67 (2000) 235–240.
[30] H. Maharaj, D.S. Maharaj, K.S. Saravanan, K.P. Mohanakumar, S. Daya, Metab. Brain Dis. 19 (2004) 71–77.
[31] R.T.P. Paul, A.P. McDonnell, C.B. Kelly, Hum. Psychopharmacol. Clin. Exp. 19 (2004) 477–488.
[32] L.R. Faulkner, A.J. Bard, Electrochemical Methods: Fundamental and Application, second ed., Wiley, New York, 2001.
[33] R. Bro, Chemom. Intell. Lab. Syst 38 (1997) 149–171.
[34] H.L. Wu, M. Shibukawa, K. Oguma, J. Chemom 12 (1998) 1–26.
[35] Z.P. Chen, H.L. Wu, J.H. Jiang, Y. Li, R.Q. Yu, Chemom. Intell. Lab. Syst 52 (2000) 75–86.
[36] A.L. Xia, H.L. Wu, D.M. Fang, Y.J. Ding, L.Q. Hu, R.Q. Yu, J. Chemom 19 (2005) 65–76.
[37] E. Sanchez, B.R. Kowalski, Anal. Chem. 58 (1986) 496–499.
[38] E. Sanchez, B.R. Kowalski, J. Chemom 1 (1990) 29–45.
[39] M. Linder, R. Sundberg, Chemom. Intell. Lab. Syst 42 (1998) 159–178.
[40] M. Linder, R. Sundberg, J. Chemom 16 (2002) 12–27.
[41] R. Tauler, Chemom. Intell. Lab. Syst 30 (1995) 133–146.
[42] H.A.L. Kiers, J.M.F. Ten Berge, R. Bro, J. Chemom 13 (1999) 275–294.
[43] W. Windig, J. Guilment, Anal. Chem. 63 (1991) 1425–1432.
[44] S. Wold, P. Geladi, K. Esbensen, J. Øhman, J. Chemom 1 (1987) 41–56.
[45] R. Bro, J. Chemom 10 (1996) 47–61.
[46] M.J. Culzoni, P.C. Damiani, A. Garcıa-Reiriz, H.C. Goicoechea, A.C. Olivieri, Analyst 132 (2007) 654–663.
[47] J. Öhman, P. Geladi, S. Wold, J. Chemom. 4 (1990) 79–90.
[48] V.A. Lozano, G.A. Iba~nez, A.C. Olivieri, Anal. Chim. Acta 610 (2008) 186–195.
[49] A.C. Olivieri, J. Chemom 19 (2005) 253–265.
[50] M.J. Culzoni, H.C. Goicoechea, A.P. Pagani, M.A. Cabezón, A.C. Olivieri, Analyst 131 (2006) 718–723.
[51] A. García Reiriz, P.C. Damiani, M.J. Culzoni, H.C. Goicoechea, A.C. Olivieri, Chemom. Intell. Lab. Syst 92 (2008) 61–70.
[52] A. García Reiriz, P.C. Damiani, A.C. Olivieri, Chemom. Intell. Lab. Syst 100 (2010) 127–135.
[53] M.B. Gholivand, A.R. Jalalvand, H.C. Goicoechea, T.h. Skov, Talanta 119 (2014) 553–563.
[54] P.H.C. Eilers, I.D. Currie, M. Durban, Comp. Stat. Data Anal 50 (2006) 61–76.
[55] N.P.V. Nielsen, J.M. Carstensen, J. Smedsgaard, J. Chromatogr. A 805 (1998) 17–35.
[56] F.S. Hillier, G.J. Liebernan, Introduction to Operations Research, McGraw-Hill, New York, 2001.
[57] D. Bylund, R. Danielsson, G. Malmquist, K.E. Markides, J. Chromatogr. A 961 (2002) 237–244.
[58] V. Pravdova, B. Walczak, D.L. Massart, Anal. Chim. Acta 456 (2002) 77–92.
[59] K. Kaczmarek, B. Walczak, S. de Jong, B.G.M. Vandginste, Acta Chromatogr. 15 (2005) 82–96.
[60] S. Thiagarajan, T.H. Tsai, S.M. Chen, Biosens. Bioelectron. 24 (2009) 2712–2715.
[61] M.G. Sullivan, B. Schnyder, M. Bartsch, D. Alliata, C. Barbero, R. Imhof, R. Kotz, J. Electrochem. Soc. 147 (2000) 2636–2643.
[62] M.G. Sullivan, R. Kotz, O. Haas, J. Electrochem. Soc. 147 (2000) 308–317.

[63] S. Yamazaki, Z. Siroma, T. Ioroi, K. Tanimoto, K. Yasuda, Carbon 45 (2007) 256–262.
[64] N.R. Vettorazzi, L. Sereno, M. Katoh, M. Ota, L. Oteroa, J. Electrochem. Soc. 155 (2008) 110–115.
[65] A. Braun, M. Bartsch, B. Schnyder, R. Kotz, O. Haas, H.G. Haubold, G. Goerigk, J. Non-Cryst. Solid. 260 (1999) 1–14.
[66] D.M. Haaland, E.V. Thomas, Anal. Chem. 60 (1988) 1193–1202.
[67] D.M. Haaland, E.V. Thomas, Anal. Chem. 60 (1988) 1202–1208.
[68] W. Windig, J. Guilment, Anal. Chem. 63 (1991) 1425–1432.
[69] R. Bro, Multiway Analysis in the Food Industry, Doctoral Thesis, University of Amsterdam, Amsterdam, the Netherlands, 1998.
[70] R. Bro, C.A. Andersoon, H.A.L. Kiers, J. Chemom. 13 (1999) 295–309.
[71] H.A.L. Kiers, J.M.F. Ten Berge, R. Bro, J. Chemom 13 (1999) 275–294.
[72] A.G. Gonzalez, M.A. Herrador, A.G. Asuero, Talanta 48 (1999) 729–736.
[73] J.A. Arancibia, G.M. Escandar, Talanta 60 (2003) 1113–1121.